JACS
JOURNAL OF THE AMERICAN CHEMICAL SOCIETY

Communication

pubs.acs.org/JACS

Cell-Permeant Large Stokes Shift Dyes for Transfection-Free Multicolor Nanoscopy

Alexey N. Butkevich,*,# Gražvydas Lukinavičius,*,# Elisa D'Este, and Stefan W. Hell

Department of NanoBiophotonics, Max Planck Institute for Biophysical Chemistry, Am Fassberg 11, 37077 Göttingen, Germany

Supporting Information

ABSTRACT: We designed cell-permeant red-emitting fluorescent dye labels with >140 nm Stokes shifts based on 9-iminoanthrone, 9-imino-10-silaxanthone, and 9-imino-10-germaxanthone fluorophores. The corresponding probes selectively targeting mitochondria, lysosomes, and F-actin demonstrate low toxicity and enable stimulated emission depletion (STED) nanoscopy in neurons, human fibroblasts, U2OS, and HeLa cells. In combination with known small Stokes shift dyes, our probes allow live-cell three-color STED nanoscopy of endogenous targets on popular setups with 775 nm STED wavelength.

Multicolor super-resolution fluorescence microscopy or nanoscopy is a valuable method for observing interactions between intracellular structures and biomolecules, as well as tracking dynamic processes in cells.[1,2] Initially, fluorescence nanoscopy of living cells relied mainly on fluorescent proteins, necessitating genetic modifications of organisms or cells. Small-molecule ligands with nanoscopy-compatible fluorophores, targeting specific proteins or organelles, avoid these difficulties.[3]

In recent reports, a number of bright green- to far-red-emitting fluorophores suitable for nanoscopy have been designed and employed as live-cell fluorescent markers.[4−6] Several dye combinations permitting two-color imaging with <60 nm resolution were identified. For example, simultaneous two-color stimulated emission depletion (STED) microscopy with a single pulsed ∼770 nm de-excitation laser was achieved by combining fluorophores excitable at ∼580 and ∼640 nm.[7] In living cells, this imaging scheme was realized with markers such as 580R or 580CP together with SiR, 640SiRH, GeR, or 630GeRH dyes.[2b,4,6a,8] The implementation of additional imaging channels with known live-cell dyes requires sophisticated techniques such as hyperspectral detection[1,9] or fluorescence lifetime recording.[10] A straightforward solution for introducing a third channel on the widely available nanoscopes with 775 nm STED wavelength relied on using large Stokes shift (LSS) labels, as demonstrated on fixed samples.[11] A LSS dye can be spectrally separated from small Stokes shift dyes on the basis of the excitation and/or emission wavelengths, and this selectivity allows an easy implementation of an additional color channel into an established two-color detection scheme employing two small Stokes shift labels. However, LSS dyes for live-cell labeling have still been missing.

Therefore, we focused our efforts on the development of LSS fluorophores capable of penetrating intact plasma membranes of living cells. Besides, they should be compatible with the popular 775 nm STED wavelength. Following the recent report by the Klán group[12] and an earlier work of Wu and Burgess,[13] we had identified 9-aminopyronin scaffold as a promising LSS analog of rhodamine. Substitution of the bridging oxygen with a 14 group element[14] allowed us to develop several selective and cell-permeant LSS probes based on these fluorophores and establish a three-color live-cell imaging scheme for standard STED microscopes.

To this end, we synthesized four 9-iminoanthrone dyes with a group in the 10-position varying between CMe_2, $GeMe_2$, $SiMe_2$, and SO_2 (Figure 1, i) and bearing a protected primary

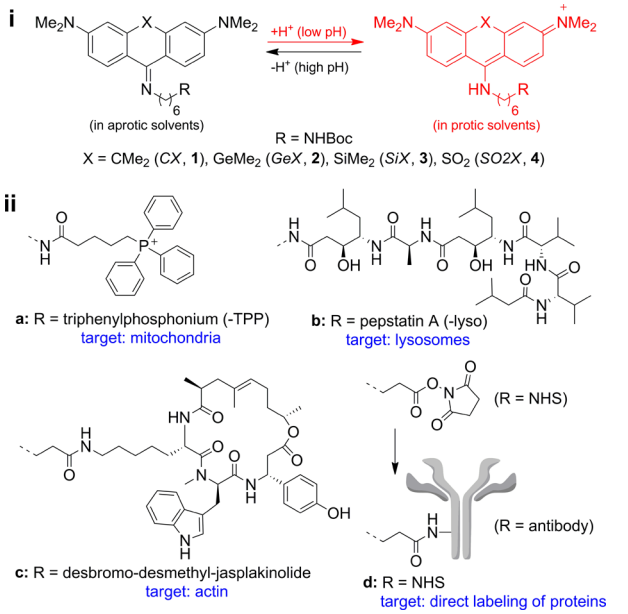

Figure 1. Chemical structures of LSS probes. (i) Protonation−deprotonation behavior responsible for the environment sensitivity of the dyes **1**−**4**. (ii) Ligands **a**−**d** for labeling of intracellular structures.

amino group or carboxylic acid for conjugation to a suitable ligand (Figure S1). Three of them, based on 9-iminoanthrone (CX, **1**), 9-imino-10-germaxanthone (GeX, **2**), and 9-imino-10-silaxanthone (SiX, **3**) fluorophores, demonstrated similar absorption and emission bands, with Stokes shifts of 140−165 nm (Table 1 and Figure S2), good photostability (Figure S3), high emission quantum yields in aqueous buffers, and

Received: June 20, 2017
Published: August 28, 2017

DOI: 10.1021/jacs.7b06412
J. Am. Chem. Soc. 2017, 139, 12378−12381

Table 1. Photophysical Properties of Dyes 1−4, Measured in 10% Methanol/PBS 7.4 (unless Otherwise Indicated)[a]

dye	λ_{max}, nm absorption (ε, M^{-1} cm^{-1})	λ_{max}, nm emission (Φ_{fl})	Stokes shift, nm	fluorescence lifetime, ns
CX (1)	459 (28000)	599 (0.55)	140	3.2
GeX (2)	454 (24000)	618 (0.17)	164	1.2
SiX (3)	458 (17000)	623 (0.28)	165	1.9
SO_2X (4)	509 (13000)[b]	647 (0.15)[b]	138	1.2[c]

[a]ε, extinction coefficient; Φ_{fl}, absolute fluorescence quantum yield. [b]In 10% acetonitrile/H_2O, [c]In 30% acetonitrile/H_2O.

fluorescence lifetimes varying by ∼1 ns. Their fluorescence emission was found to strongly decrease in nonpolar solvents and at pH > 8 (Figures S4 and S5). In pure water, loss of emission (but not absorption) was observed due to aggregation of all dyes except CX (**1**). On the contrary, the 9-imino-10,10-dioxido-9*H*-thioxanthone based dye (SO_2X, **4**) demonstrated fluorescence and intense absorption in the range >350 nm only in acidic media (pH < 5). This behavior suggested a protonation/deprotonation-based mechanism for environment sensitivity of iminoanthrone dyes (Figure 1, i). Indeed, the calculated values for the excitation maxima of the corresponding model 9-(methylimino)anthrones and their protonated forms (at the APFD/6-311++G(2d,p) level of theory) matched their experimental absorption maxima within 25 nm, with consistent overestimation of λ_{max} for imines and underestimation for iminium forms (Figure S6 and Table S1).

For intracellular targeting of the proposed fluorescent dyes, we selected two different strategies: membrane potential-based targeting for directing to mitochondria and protein−ligand interaction for selective labeling of lysosomes and cytoskeleton (Figure 1, ii). Accumulation of lipophilic cations, in particular of triphenylphosphonium (TPP) salts,[15] in mitochondria is driven by the negative potential of the inner mitochondrial membrane. Weakly basic pH of the mitochondrial matrix (about 7.9)[16] limited the LSS fluorophore choice to dyes **1**−**3** (Figures S5 and S7). All three TPP conjugates **1a**−**3a** provided high-contrast images of mitochondria (Figure S8) verified by perfect colocalization with MitoTracker Orange (Figure S9).

Pepstatin A is a known potent non-covalent inhibitor of the lysosomal protease cathepsin D (IC_{50} = 10 nM).[17] All pepstatin-derived probes (**1b**−**4b**) showed fluorescence increase upon pepsin binding (Figure S10a), were functionally active and inhibited BSA hydrolysis by pepsin (Figure S10b). The apparent K_d values of the probes **1b**−**3b** lay in the range of 40−50 nM (Table S2 and Figure S10c,d) and compared favorably to the 174 ± 27 nM value obtained for SiR-lysosome.[6a] In living human fibroblasts treated with 2 μM pepstatin A conjugates (**1b**−**4b**), the acidic compartments of lysosomes were stained brightly and selectively with GeX-lyso (**2b**) and SiX-lyso (**3b**) probes (Figure S11). Both LSS probes colocalized with CellLight Lysosomes-RFP (Figure S12). CX-lyso probe **1b** demonstrated some off-target staining of mitochondria, while no specific signal was observed for SO_2X-derived probe **4b**, and SO_2X fluorophore was excluded from further tests.

Based on these experiments, we identified GeX and SiX fluorophores as the most suitable for the development of further selective ligands, and SiX was preferred on the grounds of its higher emission quantum yield (Table 1). Jasplakinolide-derived SiX-actin probe **3c** for cytoskeletal F-actin[17,18] and amino-reactive ester SiX-NHS (**3d**) for antibody labeling were then prepared.

Prior to the live-cell nanoscopy studies, we identified threshold concentrations below which our probes were not affecting the population distribution over cell cycle, a critical parameter reflecting cell viability and proliferation (Figure 2a).

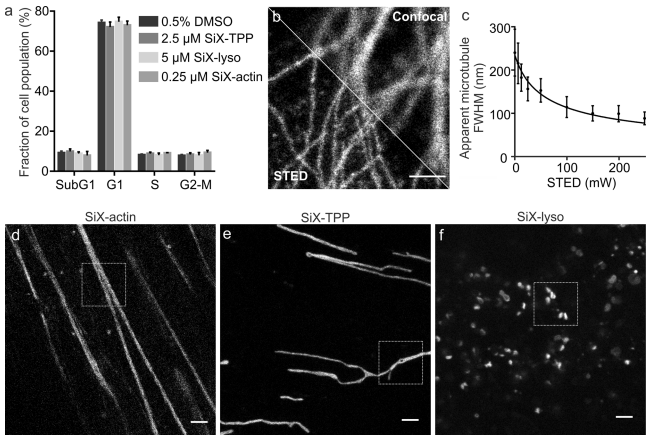

Figure 2. Performance of SiX probes targeted to different cellular organelles. (a) Percentage of cells with different measured DNA content after 24 h treatment with indicated probes vs DMSO vehicle, corresponding to cell cycle phases: G1, S, G2, and M. Cells containing less DNA than haploid (SubG1) are considered non-viable. Data are presented as mean with standard deviation, $N = 4$. For the results of t test, see Table S3. (b) Confocal and STED images of fixed human fibroblasts stained with primary mouse anti-α-tubulin and SiX-labeled secondary sheep anti-mouse antibodies. (c) Dependence of microtubule apparent thickness FWHM on the de-excitation power applied. (d−f) STED images of living human fibroblasts stained with (d) 0.25 μM SiX-actin (**3c**), (e) 2 μM SiX-TPP (**3a**), and (f) 3 μM SiX-lyso (**3b**). Dashed squares indicate zoom-in areas shown in Figure S15. Scale bars, 1 μm.

TPP probes showed little influence on cell cycle below 2.5 μM over 24 h, comparable to previous results on fluorescent TPP conjugates.[19] The lysosomal probes displayed no detectable toxic effects within the tested range; nevertheless, high concentrations (>5 μM) of these probes might influence the morphology of lysosomes and should be avoided.[20] SiX-actin **3c** altered the cell viability in sub-micromolar concentrations (above 0.5 μM), similarly to SiR-actin probe (Figures 2a and S13).[6b] Note that the following imaging experiments were carried out below the established cytotoxicity threshold.

The efficiency of SiX de-excitation was estimated in fixed human fibroblasts treated with combination of primary mouse anti-α-tubulin and SiX-tagged secondary sheep anti-mouse antibodies. We were able to reach an average apparent microtubule full-width at half-maximum (FWHM) of 88 ± 15 nm at full de-excitation laser power (250 mW entering objective, Figure 2b,c). The fluorescent primary antibody, tagged with SiX-NHS (**3d**), was used for labeling acetylated

DOI: 10.1021/jacs.7b06412
J. Am. Chem. Soc. 2017, 139, 12378−12381

tubulin in fixed human fibroblasts. The structure of primary cilium was visualized with SiX anti-acetylated tubulin, and the inner diameter of the centriole cylinder of cilium-forming centrosomes was resolved to 143 ± 5 nm (Figure S14), comparable to the previously reported diameter of 176 ± 10 nm measured in living human fibroblasts stained with SiR-tubulin.[6b]

For single-color live-cell STED nanoscopy, human fibroblasts were stained with 0.25 μM SiX-actin (**3c**). We were able to resolve F-actin stress fibers which are not discernible using confocal microscopy (Figures 2d and S15a). With 2.5 μM SiX-TPP (**3a**), mitochondrial substructures could be resolved (Figures 2e and S15b). Similarly, lysosomes stained with 3 μM SiX-lyso (**3b**) exhibit resolution improvement in STED images (Figures 2f and S15c). Additionally, actin and lysosomes could be specifically stained in living HeLa and U2OS cells with SiX-actin (**3c**) and SiX-lyso probes (**3b**), respectively (Figure S16).

We initiated live-cell multicolor confocal and STED imaging using our LSS probes by examining their concurrent use with GFP-tagged proteins. Human fibroblasts were transduced with CellLight Talin-GFP, stained with 0.25 μM SiX-actin (**3c**) for 1 h and imaged after washing. It was possible to read both channels with two detectors simultaneously while exciting with a 485 nm laser, and correct localization of talin in the focal adhesions at the end of actin stress fibers[21] was clearly visible (Figure S17a,c). The imaging scheme was further expanded to four colors (3× STED and 1× confocal) with the introduction of two additional markers: MitoTracker Orange CM-H2TMRos and GeR-tubulin[4] (Figure S17b,d). Four structures were localized, demonstrating the expected positioning of cytoskeleton and mitochondria. We also succeeded in imaging genetically unmodified human fibroblasts by three-color staining with SiX-lyso, 580CP-actin, and SiR-tubulin;[6b] lysosome movement along the microtubules could also be recorded (supplementary video). Furthermore, all three mitochondrial LSS probes (**1a**–**3a**) supported four-color imaging when applied in combination with 580CP-actin, GeR-tubulin,[4] and a plasma membrane and endosomal marker wheat germ agglutinin (WGA) labeled with Alexa Fluor 488 (Figures 3a,b and S18). Interestingly, we found that some endosomes and mitochondria share the same microtubule (Figure 3c).

Finally, we demonstrated the application of the new LSS probes to transfection-free four color staining of living rat hippocampal neurons using the combination of CX-TPP (**1a**), Alexa Fluor 488-labeled secondary antibody against a primary anti-neurofascin antibody, 580CP-actin, and GeR-tubulin.[4] Neurofascin, a marker for the axon initial segment, conveniently allowed an easy identification of axons.[22] The ubiquitous periodic organization of the actin cytoskeleton[23] perpendicular to microtubule cables was clearly visible, as well as mitochondria localized along the microtubule network (Figure 3d).

In summary, we introduced a series of new LSS probes based on iminoanthrone scaffolds suitable for live-cell imaging of lysosomes, mitochondria, and actin, as well as for immunostaining, at different physiological pH levels. The probes are cell-permeant, compatible with STED nanoscopy, and nontoxic at the recommended concentrations. The iminoanthrone dyes enable, for the first time, in combination with our previously introduced live-cell 580CP[8], GeR[4], and SiR[6a,b] labels, far-red three-color live nanoscopy with widely available 775 nm STED microscopes. Tuning the STED wavelength and power for a particular dye combination will allow further optimization of resolution. The new probes are particularly suitable for dual-color imaging with GFP fusion proteins and a single laser excitation source, resulting in reduced bleaching and permitting simultaneous signal readout in two channels. Their wide applicability opens up further exciting opportunities for live- and fixed-cell multicolor imaging with standard fluorescence microscopes as well as other nanoscopy methods.

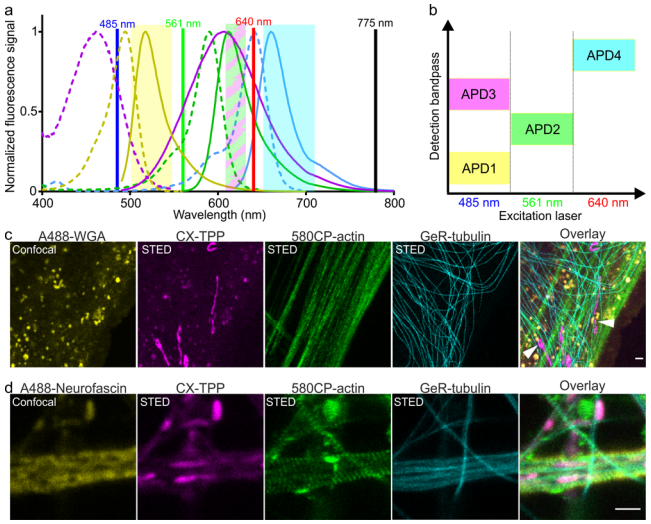

Figure 3. Four-color microscopy with CX-TPP probe. (a) Normalized absorption and emission spectra of the dyes Alexa Fluor 488 (yellow), CX (magenta), 580CP (green), and GeR (cyan) utilized for simultaneous multicolor imaging, related laser lines (solid vertical lines), and detection windows (transparent rectangles). De-excitation laser (black line) is set at 775 nm. (b) Excitation/detection scheme used for four-color imaging. (c) Four-color image of living human fibroblasts stained with 1 μM 580CP-actin, 2 μM GeR-tubulin, 2 μM CX-TPP (**1a**), and 5 μg/mL Alexa Fluor 488-WGA conjugate for 1 h at 37 °C in DMEM growth media (acquired in DMEM growth media after washing two times with HBSS). White arrowheads indicate microtubule sites co-occupied by mitochondria and endosomes. (d) Four-color image of living rat hippocampal neurons (16 DIV) stained with 1 μM 580CP-actin, 2 μM GeR-tubulin, 0.5 μM CX-TPP (**1a**) for 1 h at 37 °C, followed by anti-neurofascin and anti-mouse Alexa Fluor 488 labeling for 5 min and 30 s, respectively. Scale bars 1 μm.

■ ASSOCIATED CONTENT

Supporting Information

The Supporting Information is available free of charge on the ACS Publications website at DOI: 10.1021/jacs.7b06412.

Synthetic procedures and characterizations of the compounds, including Figures S1–S18 and Tables S1–S3 (PDF)

Supplementary video: three-color STED movie of living human fibroblasts stained with 2 μM SiX-lyso, 5 μM 580CP-actin, and 5 μM SiR-tubulin (AVI)

■ AUTHOR INFORMATION

Corresponding Authors

*alexey.butkevich@mpibpc.mpg.de

*grazvydas.lukinavicius@mpibpc.mpg.de

ORCID

Gražvydas Lukinavičius: 0000-0002-7176-1793

Stefan W. Hell: 0000-0002-9638-5077

DOI: 10.1021/jacs.7b06412
J. Am. Chem. Soc. 2017, 139, 12378–12381

Author Contributions

[#]A.N.B. and G.L. contributed equally to this work.

Notes

The authors declare no competing financial interest.

■ ACKNOWLEDGMENTS

The authors acknowledge Jan Seikowski, Jens Schimpfhauser, and Jürgen Bienert for assistance with synthesis and characterization of the probes, Dr. Shamil Nizamov (Abberior GmbH, Göttingen) for a sample of Abberior STAR 470SXP dye, and Dr. Mariano L. Bossi for helpful discussions. G.L. is grateful to the Max Planck Society for the Nobel Laureate Fellowship award. The authors thank Dr. Dirk Kamin, Dr. Sebastian Schnorrenberg, and Tanja Gilat for technical assistance and acknowledge Dr. Vladimir N. Belov and Jaydev Jethwa for proofreading the manuscript.

■ REFERENCES

(1) Winter, F. R.; Loidolt, M.; Westphal, V.; Butkevich, A. N.; Gregor, C.; Sahl, S. J.; Hell, S. W. *Sci. Rep.* **2017**, *7*, 46492.

(2) (a) Bottanelli, F.; Kilian, N.; Ernst, A. M.; Rivera-Molina, F.; Schroeder, L. K.; Kromann, E. B.; Lessard, M. D.; Erdmann, R. S.; Schepartz, A.; Baddeley, D.; Bewersdorf, J.; Toomre, D.; Rothman, J. E. *Mol. Biol. Cell* **2017**, *28*, 1676−1687. (b) Bottanelli, F.; Kromann, E. B.; Allgeyer, E. S.; Erdmann, R. S.; Wood Baguley, S.; Sirinakis, G.; Schepartz, A.; Baddeley, D.; Toomre, D. K.; Rothman, J. E.; Bewersdorf, J. *Nat. Commun.* **2016**, *7*, 10778. (c) Hell, S. W.; Sahl, S. J.; Bates, M.; Zhuang, X.; Heintzmann, R.; et al. *J. Phys. D: Appl. Phys.* **2015**, *48*, 443001. (d) MacDonald, L.; Baldini, G.; Storrie, B. *Methods Mol. Biol.* **2015**, *1270*, 255−75. (e) Erdmann, R. S.; Takakura, H.; Thompson, A. D.; Rivera-Molina, F.; Allgeyer, E. S.; Bewersdorf, J.; Toomre, D.; Schepartz, A. *Angew. Chem., Int. Ed.* **2014**, *53*, 10242−6.

(3) Xue, L.; Karpenko, I. A.; Hiblot, J.; Johnsson, K. *Nat. Chem. Biol.* **2015**, *11*, 917−923.

(4) Butkevich, A. N.; Belov, V. N.; Kolmakov, K.; Sokolov, V. V.; Shojaei, H.; Sidenstein, S. C.; Kamin, D.; Matthias, J.; Vlijm, R.; Engelhardt, J.; Hell, S. W. *Chem. - Eur. J.* **2017**, DOI: 10.1002/chem.201701216.

(5) (a) Grimm, J. B.; English, B. P.; Choi, H.; Muthusamy, A. K.; Mehl, B. P.; Dong, P.; Brown, T. A.; Lippincott-Schwartz, J.; Liu, Z.; Lionnet, T.; Lavis, L. D. *Nat. Methods* **2016**, *13*, 985−988. (b) Grimm, J. B.; English, B. P.; Chen, J.; Slaughter, J. P.; Zhang, Z.; Revyakin, A.; Patel, R.; Macklin, J. J.; Normanno, D.; Singer, R. H.; Lionnet, T.; Lavis, L. D. *Nat. Methods* **2015**, *12*, 244−50 ff.

(6) (a) Lukinavičius, G.; Reymond, L.; Umezawa, K.; Sallin, O.; D'Este, E.; Göttfert, F.; Ta, H.; Hell, S. W.; Urano, Y.; Johnsson, K. *J. Am. Chem. Soc.* **2016**, *138*, 9365−8. (b) Lukinavičius, G.; Reymond, L.; D'Este, E.; Masharina, A.; Göttfert, F.; Ta, H.; Guther, A.; Fournier, M.; Rizzo, S.; Waldmann, H.; Blaukopf, C.; Sommer, C.; Gerlich, D. W.; Arndt, H. D.; Hell, S. W.; Johnsson, K. *Nat. Methods* **2014**, *11*, 731−3. (c) Lukinavičius, G.; Umezawa, K.; Olivier, N.; Honigmann, A.; Yang, G.; Plass, T.; Mueller, V.; Reymond, L.; Correa, I. R., Jr.; Luo, Z. G.; Schultz, C.; Lemke, E. A.; Heppenstall, P.; Eggeling, C.; Manley, S.; Johnsson, K. *Nat. Chem.* **2013**, *5*, 132−9.

(7) Göttfert, F.; Wurm, C. A.; Mueller, V.; Berning, S.; Cordes, V. C.; Honigmann, A.; Hell, S. W. *Biophys. J.* **2013**, *105*, L01−3.

(8) Butkevich, A. N.; Mitronova, G. Y.; Sidenstein, S. C.; Klocke, J. L.; Kamin, D.; Meineke, D. N.; D'Este, E.; Kraemer, P. T.; Danzl, J. G.; Belov, V. N.; Hell, S. W. *Angew. Chem., Int. Ed.* **2016**, *55*, 3290−4.

(9) Valm, A. M.; Cohen, S.; Legant, W. R.; Melunis, J.; Hershberg, U.; Wait, E.; Cohen, A. R.; Davidson, M. W.; Betzig, E.; Lippincott-Schwartz, J. *Nature* **2017**, *546*, 162−167.

(10) (a) Niehorster, T.; Loschberger, A.; Gregor, I.; Kramer, B.; Rahn, H. J.; Patting, M.; Koberling, F.; Enderlein, J.; Sauer, M. *Nat. Methods* **2016**, *13*, 257−62. (b) Laviv, T.; Kim, B. B.; Chu, J.; Lam, A. J.; Lin, M. Z.; Yasuda, R. *Nat. Methods* **2016**, *13*, 989−992. (c) Zhao, M.; Li, Y.; Peng, L. *Opt. Express* **2014**, *22*, 10221−32. (d) Buckers, J.; Wildanger, D.; Vicidomini, G.; Kastrup, L.; Hell, S. W. *Opt. Express* **2011**, *19*, 3130−43.

(11) Sidenstein, S. C.; D'Este, E.; Bohm, M. J.; Danzl, J. G.; Belov, V. N.; Hell, S. W. *Sci. Rep.* **2016**, *6*, 26725.

(12) Horvath, P.; Sebej, P.; Solomek, T.; Klan, P. *J. Org. Chem.* **2015**, *80*, 1299−311.

(13) Wu, L.; Burgess, K. *Org. Lett.* **2008**, *10*, 1779−82.

(14) Koide, Y.; Urano, Y.; Hanaoka, K.; Terai, T.; Nagano, T. *ACS Chem. Biol.* **2011**, *6*, 600−8.

(15) Ross, M. F.; Kelso, G. F.; Blaikie, F. H.; James, A. M.; Cocheme, H. M.; Filipovska, A.; Da Ros, T.; Hurd, T. R.; Smith, R. A.; Murphy, M. P. *Biochemistry (Moscow)* **2005**, *70*, 222−30.

(16) Llopis, J.; McCaffery, J. M.; Miyawaki, A.; Farquhar, M. G.; Tsien, R. Y. *Proc. Natl. Acad. Sci. U. S. A.* **1998**, *95*, 6803−8.

(17) Chen, C. S.; Chen, W. N.; Zhou, M.; Arttamangkul, S.; Haugland, R. P. *J. Biochem. Biophys. Methods* **2000**, *42*, 137−51.

(18) (a) Milroy, L. G.; Rizzo, S.; Calderon, A.; Ellinger, B.; Erdmann, S.; Mondry, J.; Verveer, P.; Bastiaens, P.; Waldmann, H.; Dehmelt, L.; Arndt, H. D. *J. Am. Chem. Soc.* **2012**, *134*, 8480−6. (b) Bubb, M. R.; Senderowicz, A. M.; Sausville, E. A.; Duncan, K. L.; Korn, E. D. *Biochemistry* **1994**, *269*, 14869−71.

(19) Tan, K. Y.; Li, C. Y.; Li, Y. F.; Fei, J.; Yang, B.; Fu, Y. J.; Li, F. *Anal. Chem.* **2017**, *89*, 1749−1756.

(20) Lee, S.; Sato, Y.; Nixon, R. A. *J. Neurosci.* **2011**, *31*, 7817−30.

(21) Kost, B.; Spielhofer, P.; Chua, N. H. *Plant J.* **1998**, *16*, 393−401.

(22) Hedstrom, K. L.; Xu, X.; Ogawa, Y.; Frischknecht, R.; Seidenbecher, C. I.; Shrager, P.; Rasband, M. N. *J. Cell Biol.* **2007**, *178*, 875−86.

(23) D'Este, E.; Kamin, D.; Göttfert, F.; El-Hady, A.; Hell, S. W. *Cell Rep.* **2015**, *10*, 1246−51.

DOI: 10.1021/jacs.7b06412
J. Am. Chem. Soc. 2017, 139, 12378−12381